communications earth & environment

Article

A Nature Portfolio journal

https://doi.org/10.1038/s43247-025-02101-x

Lagrangian coherent structures influence the spatial structure of marine food webs

Jacquelyn M. Veatch[1,2] ✉, Matthew J. Oliver[3], Erick Fredj[4], Hank Statscewich[5], Kim Bernard[6], Ashley M. Hann[6,7], Grant Voirol[3], Heidi L. Fuchs[1], William R. Fraser[8] & Josh T. Kohut[1]

The patchy distribution of prey in marine environments has a large effect on upper trophic level foraging strategies and distributions. While currents can disperse or concentrate low-motility plankton into patches that reflect the dynamic fluid environments they inhabit, it remains unclear whether surface flows affect motile zooplankton. Here, we used an in-situ optical dataset to detect phytoplankton patches, active acoustics to observe krill, and GPS-tagged penguins to observe three levels of the food web. These data allowed us to investigate whether the local food web overlaps with small-scale surface transport patterns as evidence that dynamic flows structure marine food webs. In Palmer Deep Canyon, Antarctica, we deployed High Frequency radars to measure hourly ocean surface currents, which were subsequently applied to estimate attractive Lagrangian Coherent Structures. We found that phytoplankton patches, Antarctic krill (*Euphausia superba*), Adélie penguins (*Pygoscelis adeliae*) and gentoo penguins (*Pygoscelis papua*) were preferentially located in attracting Lagrangian Coherent Structure features. These results provide evidence that Lagrangian Coherent Structures act as hotspots for prey and associated foraging predators, thus spatially focusing the food web. Results highlight the role of small-scale currents in food web focusing and the importance of transport features in maintaining the Palmer Deep Canyon ecosystem.

Distributions of planktonic and nektonic marine organisms are continuously shaped by the dynamic ocean environments in which they reside and are typically patchy in space and time. Phytoplankton and zooplankton are both known to form discrete patches[1,2], with predators that seek out these patches of prey[3], which leads to a form of spatial control on the ecosystem known as food web focusing[4], where small scale fluid flows (hours-days and 1–100 km) structure the relationship between different trophic levels. Here, we are using the term "food web focusing" to describe transient and spatially variable prey patches, as opposed to prey aggregations associated with fixed spatial structures like seamounts[4]. Understanding the mechanisms that control "patchiness" seen in primary producers, primary consumers, and their predators requires integrating environmental observations of physical processes and community structure at relevant temporal and spatial scales[5,6]. These interactions between marine organisms and physical ocean processes are crucial to understanding their distribution within and reliance on the dynamic ocean habitat in which they reside.

Low-motility plankton with low and intermediate Reynolds numbers (Re ~10^{-2}–10^{3})[7], such as phytoplankton and zooplankton, are transported by ocean currents[8]. (Here, Reynolds numbers (Re) refer to how the fluid flows around the animals rather than how the fluid flows on its own). Foraging species with high Reynolds numbers (Re ~10^{6})[7] and greater mobility can employ various foraging strategies to seek out their zooplankton prey, which swim more slowly and are less able to move independently of ocean currents. The transport of low-motility plankton is particularly noticeable in areas with strong currents, often associated with features such as ocean fronts and eddies[9]. In order to understand distributions of phytoplankton, zooplankton, and top predators, we must investigate patterns in ocean transport.

Patterns in ocean transport can be elucidated through particle release experiments within observed ocean velocity fields. By integrating over Lagrangian particle trajectories, attracting structures are quantified within evolving velocity fields using an analysis known as Lagrangian Coherent Structures (LCS)[10]. Several types of LCS exist with different definitions of

[1]Department of Marine and Coastal Sciences, Rutgers, The State University of New Jersey, New Brunswick, NJ, USA. [2]Department of Applied Ocean Physics and Engineering, Woods Hole Oceanographic Institution, Woods Hole, MA, USA. [3]College of Earth, Ocean and Environment, University of Delaware, Lewes, DE, USA. [4]Computer Science Department, The Jerusalem College of Technology, Jerusalem, Israel. [5]College of Fisheries and Ocean Sciences, University of Alaska, Fairbanks, AK, USA. [6]College of Earth, Ocean, and Atmospheric Sciences, Oregon State University, Corvallis, OR, USA. [7]National Oceanic and Atmospheric Administration Uncrewed Systems Operations Center, Silver Spring, MD, USA. [8]Polar Oceans Research Group, Sheridan, MT, USA. ✉e-mail: jveatch@whoi.edu

"attraction" and "repulsion" to quantify the strength of transport features. In this study, we use Finite Time Lyapunov Exponents (FTLE) as a metric to identify attracting LCS, and test if these attracting LCS are acting as a hotspot for low-motility plankton. FTLE were chosen as they provide flexible integration time, allowing for the identification of ocean features at the scale of interest, and have been shown to identify transport features associated with increased phytoplankton patch presence in our study area[11]. LCS can quantify transport patterns in ocean velocities that cannot be seen by studying Eulerian velocity fields alone, allowing for the investigation of the role of transport in food web focusing.

LCS have been shown to overlap with bioactivity on different levels of the marine food web, shaping large phytoplankton blooms[12–15], correlating with the presence of middle trophic levels (fishes)[16], and appearing along the tracks of top predators[17,18]. Much of this previous work has been conducted on larger, geostrophic currents characteristic of open ocean (pelagic) ecosystems. On these scales, satellite-observed ocean color is often used to track the evolution of large phytoplankton patches and Global Positioning System (GPS) tags are used to track movements of large marine animals in relation to LCS calculated from satellite altimetry[12] or long range radars[14]. However, predator and prey patches likely interact at much smaller scales than measured by these systems.

Distributions of zooplankton affect prey availability for many higher trophic level predators[6] including whales[19] and commercially important fishes[20]. Therefore, a major interest in marine spatial ecology has been understanding and quantifying the factors that affect the preyscape of a marine ecosystem. While both phytoplankton and predators have been associated with attractive LCS features, the relationship between zooplankton and LCS are more difficult to obtain as they require in-situ acoustic measurements and/or net tows, and the factors that influence their distribution can be driven by both zooplankton behavior and advection.

Many of the studies linking LCS to top predators assume that, similarly to phytoplankton, zooplankton are also concentrated by attractive LCS features, though these assumptions are typically made without coincident zooplankton measurements. The few studies that have linked zooplankton to LCS were conducted over relatively large scales using data from mesoscale ocean model output[21,22] and long-range (low frequency) radars[23]. These findings suggest links between zooplankton biomass and the presence of LCS at scales of days to weeks and tens of kilometers. Other studies have associated zooplankton distributions with mesoscale eddy kinetic energy[24], tidal cycles phases[25,26], and wind events[25,27] suggesting connections between ocean dynamics and zooplankton swarms. Larger top predators such as whales have also been shown to select for LCS-identified prey concentrating features over larger scales[23]. However, predators likely seek prey patches on much smaller scales[28,29], meaning these coarser-scale associations between LCS and predators could be averages of finer scale processes. Using an Antarctic submarine canyon as our natural laboratory, we resolved the food web at scales of hours to days across spatial scales of hundreds of meters to kilometers and observed transport features experienced by near-shore patches of phytoplankton, zooplankton and associated predators. To our knowledge, the following study is the first, to the best of our knowledge, to include concurrent high-resolution observations of zooplankton, phytoplankton and upper trophic predators in relation to LCS-identified ocean features.

For this study, we focus on the local food web of Palmer Deep Canyon along the Western Antarctic Peninsula (WAP). Here, Antarctic krill (*Euphausia superba*, hereafter referred to as krill) serve as a keystone species and a major food source for marine predators including whales, seals, and penguins[27,30–34]. Local Adélie (*Pygoscelis adeliae*) and gentoo (*Pygoscelis papua*) penguins are both central place foragers, meaning they return to a nest after each foraging trip, with overlapping foraging areas centered over Palmer Deep Canyon (Fig. 1b). Penguin populations in Palmer Deep Canyon have persisted for hundreds of years[35–37], their diets dependent at least in part on the elevated biomass of krill[38] that persists here in relation to neighboring regions[37,39,40], establishing Palmer Deep Canyon as a "biological hotspot". Consequently, Palmer Deep Canyon's ecosystem hinges on the availability of krill as the trophic link between phytoplankton at the base of the food web and higher predators[41]. In this study, we investigate current-driven controls on the distributions of phytoplankton patches and krill

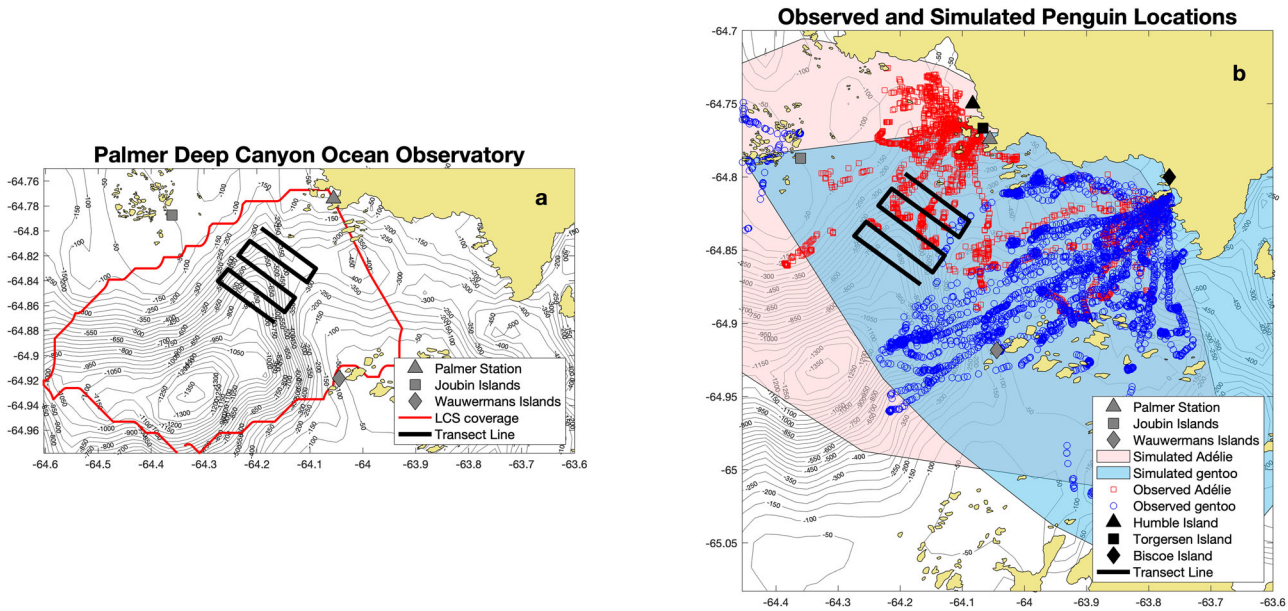

Fig. 1 | Ocean observatory around Palmer Deep Canyon. a Palmer Deep Canyon study region with the location of the three High Frequency Radars shown with polygons and the area of LCS results contoured. Within the LCS footprint is the transect line of the active acoustic survey used to detect krill and optical survey used to detect phytoplankton patches. Canyon bathymetry is contoured in 50 m isobaths. **b** Penguin positions observed with GPS tags for Adélie (red squares) and gentoo (blue circles) penguins. Convex hulls of simulated Adélie and gentoo penguins are shown in red and blue respectively, the smallest convex polygon that contains the set of points produced by the simulated penguin tracks. Penguin nests are shown in black polygons. Adélie breeding colonies are located on Humble Island, Torgerson Island, and Biscoe Island, and gentoo breeding colonies on Biscoe Island. Transect line for the surveys that observed krill swarms and phytoplankton patches is shown with a solid black line. Canyon bathymetry is shown in contours of 50 m isobaths. Note that the seemingly strait penguin tracks are likely penguins returning to their nests after satiation.

swarms at the scales of penguin foraging through the use of a multi-platform ocean observing system (Fig. 1a). Integration of multiple observing platforms provides the rare opportunity to analyze the overlapping physical processes and trophic interactions on time and space scales relevant to understanding the physical mechanisms that concentrate high density patches of prey that predators use to efficiently forage.

When integrating both biological and physical observations of an ecosystem, it is important to investigate them at the appropriate space and time scales[42]. Palmer Deep Canyon is a coastal system, characterized by submesoscale ocean currents, strong tidal influences, and short (2–7 days) surface residence times[43]. Similarly, phytoplankton patches have been shown to move through this system quickly (6 h decorrelation)[11], and most penguin foraging trips are between 6 and 24 h[44]. Previous work has established Palmer Deep Canyon as a fast-moving oceanic habitat, characterized by dynamic physical conditions and a similarly variable biological ecosystem. In this study, we determine if the distribution of krill and foraging penguins at these shorter time and space scales show similar association with LCS-identified transport features as previously observed with phytoplankton[11], suggesting small-scale and current-driven controls on food web focusing. The present study maps each level of the food web onto dynamic ocean currents at resolutions that resolve interactions between near-shore creatures and complex coastal flow, providing a unique opportunity to deepen our understanding of potential small-scale physical mechanisms of spatial ecology.

Results

Dynamic feature mapping with Lagrangian Coherent Structures

In this study we used a high-resolution High Frequency Radar (HFR) network to calculate attracting FTLE, projected at the temporal and spatial resolution of inputted HFR data (1 h, 1 km). FTLE is a metric used to characterize the Lagrangian structure in fluid flows. It measures the rate of separation of initially close particles over a finite time interval, providing insights into the stability and chaotic behavior of the flow (see section 5.7 for details). FTLE maps were calculated each hour with a 1 km spatial resolution (Fig. 2 and Supplementary Movie 1), the same spatial and temporal resolution as the HFR velocity field data. Higher values of LCS indicated a higher influence on the attraction of nearby drifting particles. This analysis produced a time resolved 2-dimensional field of attracting features.

Phytoplankton patches occuring in transport features

Phytoplankton patches were observed with an ACROBAT, a towed instrument that undulates between the surface and ~50 m depth (see Section 5.3 for details), outfitted with a Wetlabs Ecopuck optical sensor (chlorophyll-a, CDOM fluorescence, and optical backscatter at 700 nm) and a fast-sampling (16 Hz) Seabird 43 FastCAT CTD (conductivity, temperature, and pressure) following transect lines within the HFR footprint (Fig. 1a). MLD was calculated as the depth of maximum buoyancy frequency for each profile[11,45] using data collected via the towed ACROBAT. Phytoplankton patches were determined following methods in Veatch et al.[11] as profiles with an integrated mixed layer backscatter greater than a threshold, and re-analyzed in this study for direct comparison with krill and penguin foraging observations (Section 5.3, Supplementary Fig. 2).

Previous results found phytoplankton patches were associated with higher FTLE values (indicative of stronger attracting features) than a null model[11]. The distribution of FTLE values associated with phytoplankton patches are shifted towards higher FTLE values, peaking around 0.3 hr^{-1} while the distribution of FTLE values associated with randomized phytoplankton patches (null model) were more symmetrical, peaking around 0.22 hr^{-1} (Fig. 3). Randomized phytoplankton patches were created by generating survey transects in random locations and associating them with LCS (see section 5.6 for details). The distribution of FTLE values associated with observed phytoplankton patches were significantly higher than those of randomized phytoplankton patches (Fig. 3a), according to a one-sided Kolmogorov-Smirnov (KS) test ($p = 0.01187$) which tests whether one sample distribution tends to have greater values than the other. Results were the same when the null model was confined to the area of the observed transect (see section 5.6 for details) passing a one-sided KS test ($p = 2.54e{-}11$).

Krill swarms occuring in transport features

Krill swarms (Fig. 4) were concurrently mapped using active acoustics during small boat surveys within the HFR footprint (Fig. 1a) during daytime surveys. The small boat was equipped with a hull-mounted EK80. Krill were acoustically detected and parameterized following methods previously used in Palmer Deep Canyon[28,46–48]. Mixed layer depth (MLD) was also observed using a CTD aboard a towed ACROBAT instrument (see Sections 3.2, 5.3). Of the 1749 total krill swarms detected, 687 (~39%) were observed above the MLD. A null model representing random distribution of krill aggregations across the survey area was created to compare to observations.

Observed krill swarms as well as randomized krill swarms from a null model were matched in space and time with FTLE. The density distributions of FTLE for krill swarms (above the MLD, below the MLD, and total) are skewed towards higher FTLE with the peak around 0.35 hr^{-1} for krill above the MLD, 0.33 hr^{-1} for krill below the MLD, and 0.35 hr^{-1} for all krill swarms (Fig. 3b). In contrast, the density distributions of FTLE for randomized krill swarms is relatively symmetrical in shape, peaking at a lower value around 0.25 hr^{-1}. A KS test between density distributions of FTLE for observed and randomized krill swarms showed that the distribution of true krill swarms is skewed toward higher FTLE values compared to randomized krill swarms. There was a significant difference between total krill swarms and randomized krill swarms ($p = 9.57e{-}14$). This was also true for krill swarms both above and below the MLD ($p = 0.0028$ and $p = 5.56e{-}12$, respectively) (Fig. 3b). When all krill swarms were compared to null model confined to the area of the observed transect (see section 5.6 for details) results were the same, passing a one-sided KS test ($p = 7.16e{-}39$).

Adélie and gentoo penguins selecting for transport features

Penguin diving locations, tracked using Fastloc GPS archival tags, showed preference for higher values of FTLE. Similar to the krill swarms, density distributions of FTLE associated with observed Adélie penguin diving locations indicated that Adélie penguins tended to forage in regions with higher FTLE compared to the simulated Adélie penguin tracks (KS test, $p = 2.7e{-}5$). Adélie locations with dives less than 10 m deep (KS test, $p = 2.2e{-}15$) and locations with dives greater than 10 m deep (KS test, $p = 0.0017$) both showed higher density distributions of FTLE compared to null models, with 10 m representing the average MLD calculated from the towed ACROBAT instrument. Like Adélie penguins, the density distributions of FTLE associated with observed gentoo penguin diving locations was shifted towards higher FTLE values compared to randomized gentoo penguin foraging locations (KS test, $p < 1.66e{-}15$). Observed gentoo penguin foraging locations were also associated with higher FTLE values compared to randomized foraging locations for dives with maximum depths above and below 10 m ($p < 1.15e{-}13$ and $p < 9.6e{-}12$, respectively). The density distributions of FTLE for Adélie and gentoo penguins are shifted towards higher FTLE (Fig. 3c, d). In contrast, the density distributions of FTLE for simulated Adélie and gentoo penguins are relatively symmetrical in shape. For all three of these comparisons (all dives, dives shallower than 10 m, and divers deeper than 10 m), we systematically removed one penguin from the analysis and recomputed the KS test, as each sampling group was O10 penguins. The resulting distributions showed that no individual penguin was driving the shift of Adélie or gentoo penguins toward higher FTLE values (see the grey shaded area in Fig. 3c, d).

Discussion

In this study, we observed that food web focusing by small-scale currents shapes the spatial ecology of a coastal marine food web at the patch scale of foraging (hours and 100 s of meters to kilometers). Our results show that phytoplankton, krill, and penguins are found in higher attracting FTLE features (LCS), suggesting aggregation of plankton from horizontal ocean

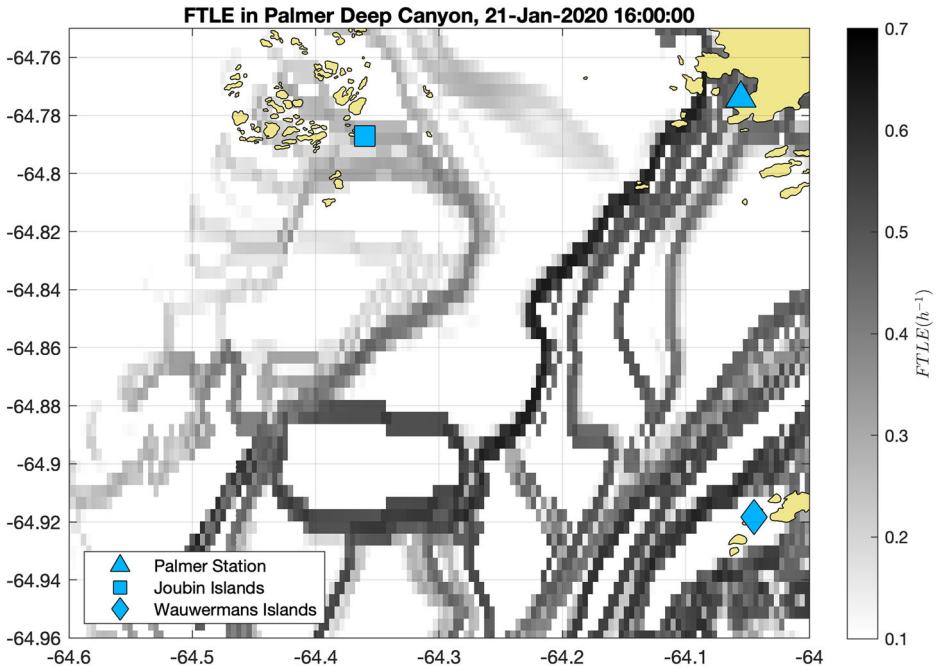

Fig. 2 | Example FTLE results calculated from High Frequency Radar observed surface currents. Locations of three HFR stations are denoted with polygons. FTLE results on January 21st 2020 at 16:00 GMT are shown in greyscale with higher FTLE values corresponding with stronger attracting ocean features.

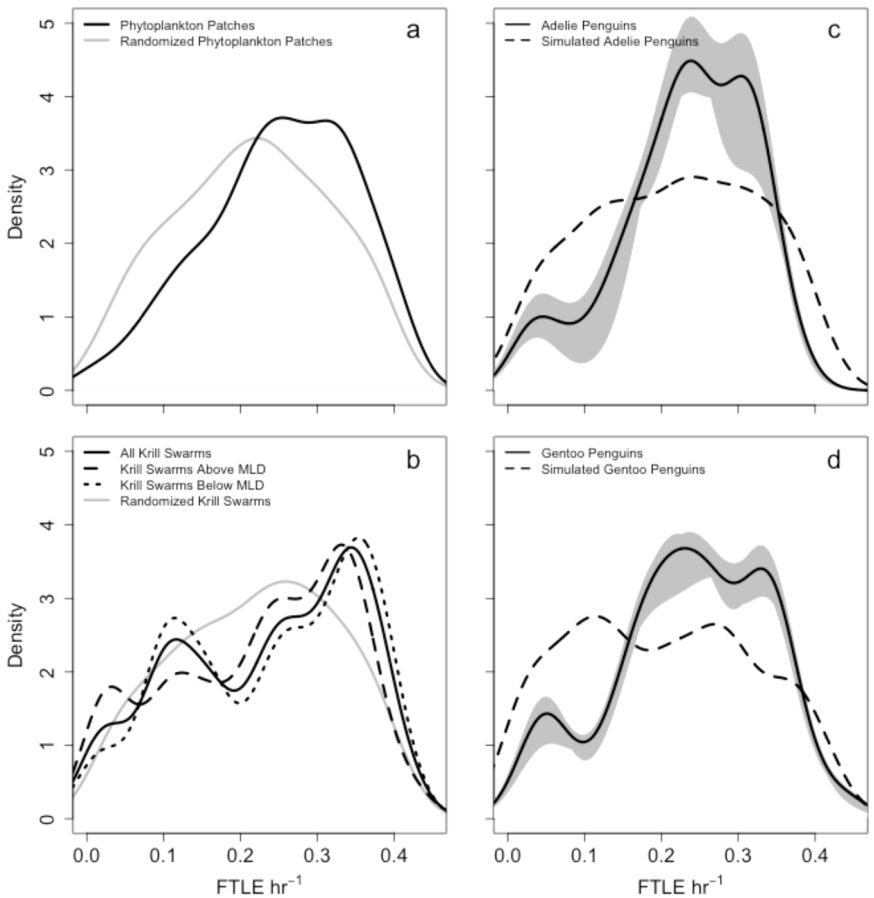

Fig. 3 | Density distributions of FTLE. a Density distributions of FTLE associated with observed phytoplankton patches (black line) and randomized phytoplankton patches (grey line) previously published in Veatch et al.[11]. Phytoplankton patch FTLE value density distribution were skewed toward higher values compared to randomized phytoplankton patches (KS test, $p = 0.01187$). **b** Density distributions of FTLE associated with observed krill swarms (solid line) above (dashed line) and below (dotted line) the mixed layer depth. All three of these distributions are skewed toward higher FTLE values than randomized krill swarms (grey line) (KS test, $p = 9.57e{-}14$, 0.0028, $5.56e{-}12$). **c** Adélie and (**d**) gentoo tagged penguin FTLE values shown in solid line and randomized penguin FTLE values with dashed line. Grey regions represent the distributions of either Adélie or gentoo penguins if individual birds were systematically excluded from the analysis. This was done to determine if an individual bird was driving the results. Both Adélie and gentoo FTLE distributions were skewed toward higher values compared to FTLE values with simulated penguins (KS test, $p = 2.7e{-}5$, $p < 1.66e{-}15$). All curves are kernel density estimates computed with a density function within the statistic package of *R*[86], with the bandwidth of the kernel smoother set to 0.03. These density curves visualize the frequency of the underlying data.

transport is an important factor in the spatial ecology of Palmer Deep Canyon and providing the first evidence, to the best of our knowledge, of LCS selection at these scales across primary producers, primary consumers, and predators.

Interactions with ocean transport from each trophic level

The three trophic levels tested in this study span a wide range of Reynolds numbers with significant differences in their behavior and in the dependence of their movement on ocean currents. The passive particles used in

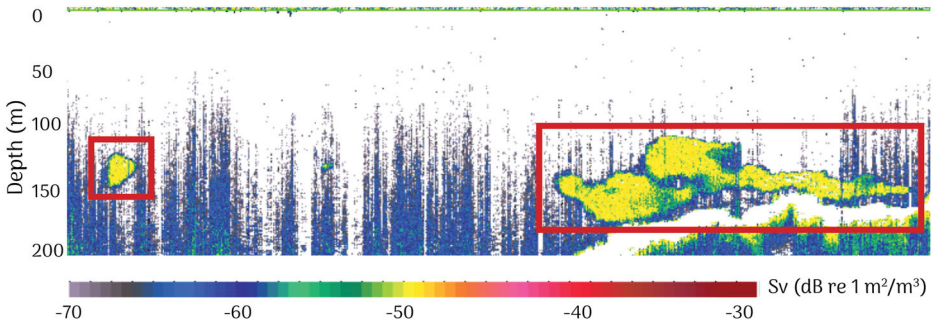

Fig. 4 | Example of acoustic detection of krill swarms. Echogram from survey (see Fig. 1a for survey path) with ACROBAT deployment. Dense yellow regions outlined in red boxes were detected as krill using a threshold of −70 to −30 dB. Raw acoustic data was processed in Echoview software, following methods of Tarling et al.[47,48] to identify krill swarms from all other backscatter.

LCS calculations most closely approximate the non-motile characteristics of phytoplankton at the scales of this study (Re ~10^{-2}, estimated from length scale[7]). The correlation between phytoplankton patches and LCS, their immobility, and their slow growth rates compared to local surface residence time[43] suggests that these patches are formed through horizontal ocean transport.

Unlike the largely passive phytoplankton cells, krill exhibit movement behavior relative to local ocean currents (Re ~10^3) and migrate vertically based on the sun angle[49], which means they can both be transported by ocean currents and swim somewhat independently of them. Our analysis used only passive particles and current velocities at the surface, yet surprisingly, high FTLE values indicated that krill both above and below the MLD were preferentially associated with surface concentrating features. Dynamics below the mixed layer are outside the scope of this study, but we can speculate why krill below the MLD would have higher FTLE values than a null model using surface particles. Krill below the MLD may have recently migrated down from within the mixed layer, and have not yet become decorrelated with surface currents. It is also possible that the velocity field below the MLD may be similar to that in the mixed layer, concentrating sub-surface krill in similar patterns to those reflected in the surface. Similarities between the surface and the sub-surface velocity fields could be driven by this region's barotropic tides[50], creating similar concentrating features in the sub-surface as in the surface velocities used to calculate FTLE. Finally, krill may be attracted to locally concentrated phytoplankton in higher FTLE values, indicating that both advection and behavior explain their affinity for LCS features with high FTLE values. Regardless of the mechanism, these results suggest that the distribution of krill in Palmer Deep is affected by food web focusing driven by small scale currents.

Foraging penguins have very high Reynolds numbers (Re ~10^6), indicating that they may move independently of currents. As a result, their distribution is expected to be most unlike the passive particles used in the LCS calculations. Results from this study show that penguin foraging behavior leads to spatial distribution in which there is more frequent penguin dives around locations with strong concentrating features (high FTLE). This suggests that while penguins may not actively seek out LCS, they are more likely to dive once they reach these features and find concentrated prey. Similar conclusions were drawn by a previous study investigating elephant seals interacting with larger scale currents[51], showing that elephant seals increase their foraging dives when at distinct oceanographic features. Unlike the elephant seals, Adélie and gentoo penguins will return straight to their nests once satiated, which creates the directed return journeys in the penguin tracks (Fig. 1b).

Penguin dives above and below the MLD, associated with stronger FTLE values, suggest that while penguins may use surface cues to initiate dives, they do not limit their foraging to the surface layer. This result is consistent with findings in krill distributions, where krill swarms both above and below the MLD were associated with strong FTLE. Penguins and other marine mammals transit near the ocean surface from where they dive to search and forage for their prey, exhibiting a variety of movement modes[52–54]. Although dive location and frequency can be quantified, little is known about the selective interactions of animals during their foraging trips that produce these patterns[55], including whether animals actively search for prey or use environmental cues associated with prey[56]. Emerging theories suggest that selection for environmental cues is likely[57], but it is unknown if Adélie or gentoo penguins respond to prey or environmental cues. Further research is needed to identify the surface cues Adélie and gentoos use to decide when to dive for prey.

Despite the wide range in the Reynolds numbers of our study species, each species showed selectivity for horizontally concentrating features (LCS) derived from passive particle trajectories. As species size and Reynolds number increases, so does the complexity of their relationship to LCS. Phytoplankton have low Reynolds numbers, and their distributions are likely dominated by ocean transport. Krill have intermediate Reynolds numbers, and their selection for LCS likely reflects a combination of physical concentration by attractive features and behavioral attraction to phytoplankton patches. Lastly, Penguins have high Reynolds numbers and behavior-driven distributions, so their selection for LCS is likely dominated by foraging behavior concentrated at krill patches. Such selectivity across species with varying Reynolds numbers demonstrates the importance of ocean transport to multiple levels of the food web.

Observations of small-scale ocean transport with Lcs

Selection by multiple levels of the food web for LCS quantified by FTLE at a 6-h integration suggests that FTLE capture transport patterns that create small-scale (sub-tidal) food web focusing. FTLE is a paired particle tracking technique, meaning that it uses relative distances between neighboring particles to quantify attraction and repulsion. This allows FTLE to quantify attracting features with little influence of the particle's starting position, unlike the single particle tracking methods[11]. FTLE also assigns scalar quantities to attracting features based on separation rate of neighboring particles (backwards in time, particle accumulation rate), allowing FTLE to account for rate of change of particle position rather than position alone. Additionally, FTLE integrate over particle trajectories, adding "memory" of particle position to the calculation of attracting features. Yet another strength of this method is the integration over time, which pairs well with the high temporal resolution of the HFR velocity data. The incorporation of relative particle motion and integration over particle trajectories makes FTLE a powerful tool for quantifying small-scale transport compared to the use of particle trajectories on their own.

FTLE patterns at these scales are highly variable in space and time, yet ubiquitous throughout the study system (Supplementary Movie 1 and Fig. 1). The null model sensitivity test showed similar results when the null model was constrained to the area closer to the observed transect rather than the entire LCS bounds (Fig. 5). Therefore, FTLE are not concentrated over the observed transect but throughout the study region. It is unknown whether penguins select their colony locations based on proximity to heightened LCS features. This study sets the groundwork for future investigations into whether coastal regions on the WAP near persistent penguin colonies have heighted FTLE activity compared to regions without such colonies.

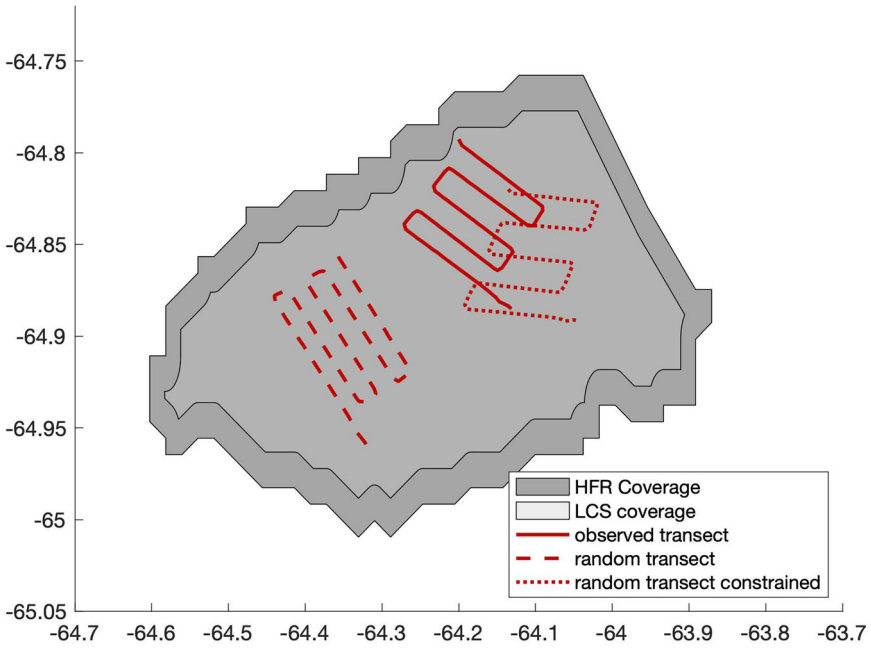

Fig. 5 | Example of null model. The area of LCS coverage is plotted in light grey, shrunk from HFR coverage (dark grey) to exclude edges of data. The transect where phytoplankton patches and krill swarms were observed is plotted with a solid red line, and one of the randomly rotated and translated transects is plotted with a dashed red line. A sensitivity test was conducted on the null model, constraining "randomly generated" transects to the northeast of the solid black line. A randomly rotated and translated transect confined to northeast of the black line is plotted with a dotted red line. Figure modified from Veatch et al.[11] Fig. 3.

In addition to identifying areas of attraction, strong FTLE will appear as horizontal transport barriers, which manifest as horizontal buoyancy gradients (fronts and edges of eddies) in ocean velocity fields. This makes areas of high FTLE oceanographically distinct from areas with low FTLE values. While attractive transport is likely to be a large reason why phytoplankton and zooplankton are associated with high FTLE values, it is unclear if Adélie and gentoo penguins are able to select for areas of high FTLE based on a learned oceanographic cue or if they are able to perceive large krill swarms and those happen to be at areas of high FTLE. Future work is needed to investigate penguin (and other forager) behavior that leads to their association with areas of high FTLE.

Limitations and caveats

There are several biological processes that limit the conclusions that can be made with these observational data. Mapping of prey, which was conducted through small boat surveys twice weekly, provides a snapshot in time of a prey field that is constantly evolving. The timing of observation within the process of food web focusing is unknown. For example, an area where there was an LCS-identified transport feature could have been observed shortly after a predator fed on a krill swarm. Our observations would show that an LCS-identified transport feature was there without presence of food web focusing, when in fact there was. Our observations could have also occurred before the ecosystem was able to respond to the presence of the LCS, perhaps showing high phytoplankton but no krill, or krill swarms but no penguin foraging. Additionally, far fewer predators (penguins) exist than prey (krill), making it more difficult to correlate predators to food web focusing events. With these caveats in mind, the patterns that were observed likely underestimate the food web focusing effect of small-scale transport.

Local and global implications

Results and conclusions from this study increase our understanding of how a coastal biological hotspot is maintained in the context of a larger marine ecosystem. Palmer Deep Canyon was once considered to be a location where phytoplankton production is driven by local upwelling[40]. Recent studies provide evidence against this, showing instead almost no stratified summertime occurrence of nutrient-rich Upper Circumpolar Deepwater in the photic zone[58]. Further, production is light limited rather than nutrient limited[59], suggesting little reliance on locally upwelled nutrient rich waters. Furthermore, a deep, recirculating eddy driven by the bathymetry of Palmer Canyon has the ability to trap krill performing diurnal vertical migration[60]. This feature may provide a seasonal reservoir of krill, which migrate to the surface, and are then aggregated in surface LCS structures. Emerging theories propose that high concentrations of phytoplankton[40] are advected from the shelf break where upwelling of nutrient-rich Upper Circumpolar Deep Water fuels phytoplankton blooms[61,62]. Future work is needed to further investigate larger scale, regional transport that reflects climate scale impacts in the WAP region. Our results further emphasize the importance of ocean transport in this system not just for local phytoplankton abundance but throughout the food web. Oceanographic transport patterns that reliably concentrate prey could be a reason penguins colonies have persisted in this region over ecological time scales[37]. As Palmer Deep Canyon and other ecosystems along the WAP experience rapid warming[63–65], sustained observations are needed to determine if these transport patterns that local food webs rely on will change. Future work must also investigate the fate of the sources of plankton that are being delivered to the system in order to predict Palmer Deep Canyon's resistance to changing climate. A depletion of these sources could be detrimental to Palmer Deep Canyon's ecosystem even if transport patterns are maintained.

Selectivity of LCS calculated with short integrations by intermediate and upper trophic levels illustrates the importance of small-scale transport features in the spatial ecology of coastal systems. This not only supports the emerging theory of trophic focusing by physical ocean processes[4], but demonstrates that these processes occur on the sub-mesoscale. Correlations between LCS and phytoplankton, zooplankton, and top predators stress the importance of incorporating LCS as a covariate in predictions of spatial ecology in marine systems.

Our study provides a link between the preyscape of a coastal ecosystem and ocean transport. This relationship fills the gap in previous studies that link phytoplankton and top predators' distributions to ocean transport without considering the critical mid-trophic level zooplankton. Results also provide a useful tool for the marine ecological community to quantify ocean transport features, namely FTLE. FTLE, although more computationally complex than single particle tracking techniques such as Relative Particle Density[11,66], have been shown to quantify transport features that are selected by each level of the Palmer Deep Canyon food web, justifying their use in dynamic coastal environments. Connections between ocean movement and spatial ecology improve current understanding of how local populations use

their ocean habitats, enabling more informed conservation strategies to protect areas of prey accumulation, mitigating anthropogenic impacts on coastal ecosystems.

Methods

An ocean observatory was deployed around Palmer Deep Canyon during January-March 2020, mapping phytoplankton, zooplankton, and penguin foraging behavior onto physical ocean processes. The following section describes the small boat surveys that were conducted along a transect twice weekly to observe phytoplankton and zooplankton as well as the HFR array observations and tagged penguin measurements that overlapped with this transect.

High Frequency radar

Three High Frequency Radars were deployed around Palmer Deep Canyon, using doppler-shifted radio waves backscattered from ocean waves to produce vector maps of surface current velocities each hour. HFRs were deployed on the Joubin Islands, Wauwermans Islands, and at Palmer Station (Fig. 1). Remote sites (Joubin and Wauwermans) were each accompanied by a remote power module, described in refs. 67,68. Radial components from each radar[69] were added together with an optimal interpolation algorithm[70] and gap filled[71] as described in refs. 11,72. The resulting data product is an evolving hourly map of ocean surface currents over a 1 km spatial grid.

Calculating mixed layer depth

On the active acoustic survey transects (Fig. 1a), an ACROBAT (Autonomous Conductivity, temperature, and depth Rapidly Oscillating Biological Assessment Towed) was towed, equipped with a fast-sampling (16 Hz) Seabird FastCAT CTD (conductivity, temperature, and pressure). This instrument undulated between the surface and about 50 m depth, profiling the upper water column about every 300 m in the horizontal. For each profile, MLD was determined as the depth with the maximum buoyancy frequency following methods in Carvalho et al.[45]. MLD measurements were used to calculated mixed layer optical backscatter (Section 5.3) and to determine if krill swarms were above or below the MLD (section 5.4). ACROBAT profiles were matched with observed krill swarms in space and time, assigning a MLD to each krill swarm. If the depth of the krill swarm was shallower than the ACROBAT observed MLD, the swarm was considered to be within the mixed layer.

Optical surveys

Towed ACROBAT surveys were conducted twice weekly collecting optical measurements of the water column along transects shown in Fig. 1a. Methods for identifying phytoplankton patches with ACROBAT optical measurements followed those in Veatch et al.[11], and are explained thoroughly there. In short, the ACROBAT profiled between the surface and about 60 m, completing a profile about every 300 m of horizontal distance traveled. Profiles were determined as "within a phytoplankton patch" or "not in a phytoplankton patch" based on a daily threshold of integrated mixed layer optical backscatter. In this system, optical backscatter is a good proxy for phytoplankton biomass and avoids the problem of non-photochemical quenching that is associated with measuring phytoplankton fluorometrically. Consecutive profiles designated as "within a phytoplankton patch" were assumed to be in the same phytoplankton patch (Supplementary Fig. 2).

Each ACROBAT profile was assigned an FTLE value based on the closest FTLE grid point to the profile in space and time. Phytoplankton patches made up of multiple profiles were assigned an FTLE value based on the average FTLE value assigned to the profiles within that phytoplankton patch.

Acoustic surveys

Active acoustic surveys were conducted twice weekly using a hull-mounted SIMRAD EK80 single-beam, single frequency (120 kHz) echosounder (Kongsberg Maritime) along transects shown in Fig. 1a. The echosounder was configured with a 1 s ping rate, 512 µs pulse duration, and 24 µs sampling duration. Calibrations of the echosounder were performed in the vicinity of Palmer Deep Canyon using a tungsten sphere (diameter = 38.1 mm) during February, 2020. Acoustic data were processed in Myriax Echoview software version 11.1 following methods from Tarling et al.[47] and Tarling et al.[48]. Raw data were processed to consider the echosounder calibration and in situ ocean acoustic conditions via incorporation of onboard CTD data, and to remove background noise and other interferences via the Background Noise Removal[73] and Impulse Noise Removal[74] algorithms in Echoview. Krill were then detected using a target strength threshold of −70 dB to −30 dB[47,48] in Echoview following similar parameterization and protocols to Nardelli et al.[28] and Reiss et al.[75] (Fig. 3).

All acoustically detected krill swarms were manually reviewed before exporting the acoustic data in Nautical Area Scattering Coefficient (NASC) values, a common proxy for organism presence in acoustic measurements. NASC values were calculated per detected swarm and exported along with depth, GPS position (longitude and latitude), swarm height, swarm length, and backscatter (Sv). These methods for acoustic surveys and processing of subsequent acoustic data follow those in Hann et al.[46].

Table 1 | Tagged penguins by colony

Colony	Penguins tagged	Trips recorded
Adélie - Humble Island	12	23
Adélie - Torgersen Island	13	24
Adélie – Biscoe Island	5	13
Gentoo - Biscoe Island	14	32

Number of individual Adélie and gentoo penguins tagged per colony.

Penguin tagging

Adélie penguin colonies were located on Humble Island (64°45'S, 64°05'W), Torgersen Island (64°46'S, 64°04'W), and Biscoe Island, (64°48'S, 63°46'W), with the latter location also including a colony of gentoo penguins (Fig. 1b). Both species were double tagged with GPS tags and time-depth recorders measuring pressure at 0.5 Hz while wet. Penguins were GPS tagged with either a Lotek FastGPS (F5G 234B, 35 g), Sirtrack Fastloc 3 loggers (30 g) or igotU GT-600 (35 g, Mobile Action Technology, Taiwan). IgotU loggers were encased in adhesive-line heat shrink tubing. The time-depth recorders were either a Lotek LAT1810 (10 g) or StarOddi DST CTD (22 g). Tags were adhered to the anterior feathers on the lower dorsal area of the penguin. All protocols were carried out in accordance with the approved guidelines of the Columbia University (Assurance #AAAS2504) Institutional Animal Care and Use Committee for the 2019–2020 season. Tags were generally deployed on individuals for 2–4 days before being removed and reattached to another penguin. We tagged 30 Adélie and 14 gentoo penguins over the course of the austral summers (Table 1).

Drift in the depth data for tags was zero offset corrected using the *calibrateDepth* function in the R package diveMove[76]. Drift was not corrected for 7 deployments, as on 6 of these deployments (all Adélies, 5 Humble Island, 1 Torgersen Island) depth recordings shallower than 1 meter were not taken, and on 1 deployment (1 Adélie, Humble Island) depth recordings shallower than 5 meters were not taken. GPS data were filtered for erroneous locations based on improbable swimming speeds (>2.8 m s^{-1}). GPS location and TDR data were time matched and dives were identified using the *diveStats* function in diveMove[76].

Penguin data collection was conducted by Polar Oceans Research Group (PORG) as part of project SWARM.

Creating null models

Distribution of LCS where phytoplankton patches and krill swarms were observed in our transects were compared to those along simulated "null model" phytoplankton patches and krill swarms. The phytoplankton and krill null models were created by randomly moving the observed

distribution of phytoplankton and krill within the LCS field (Fig. 5), maintaining the observed phytoplankton patch and krill swarm size and distribution along the transect. Each of the thirteen surveys were rotated and translated 100 times, creating 100 randomized locations of each observed phytoplankton patch and krill swarm while maintaining the shape of the survey. This ensured that the survey shape did not contribute to differences found between observed and null model phytoplankton patches and krill swarms. These randomized locations make up the phytoplankton and krill null model. Methods for using the survey transect to create the null model were adapted from Veatch et al.[11].

A sensitivity study was conducted on the null model to test if the differences between the null model and observations were due to the area where the survey was conducted having more FTLE than elsewhere in the study area. A new model was created following above methodology but requiring the randomly moved transects to be within a smaller area closer to the observed transect (northeast of the black line in Fig. 5). This constrained null model produced the same results as the original null model (see Results).

Distribution of LCS selected by penguin GPS locations were compared to those along simulated "null model" penguin tracks. Penguin null models were created with simulated Brownian motion of central place foragers (simm.bb in the adehabitatLT R package)[77], having the simulated penguin tracks return to the Adélie and gentoo colonies at the end of each trip (Fig. 1b). Each day that we had overlapping penguin observed data and LCS results from HFR-observed surface currents, ten penguin trips were simulated for each species. These trips were limited to 24 h, and simulated penguin speeds were normally distributed around a mean of 4 km hr^{-1} with a maximum of 8 km h^{-1}. These limitations were set to mimic average foraging trip duration (6–24 h)[44] and swimming speeds[78] of Adélie and gentoo penguins. The Brownian motion used to create these tracks is uncorrelated. Therefore, simulated tracks represent random foragers that do not select for environmental features or remembering previous feeding locations. Simulated penguin locations were used as a null metric for all the available LCS values for non-selecting central place foragers. Methods for the creation of simulated Adélie and gentoo tracks were adapted from Oliver et al.[66].

Calculating Lagrangian Coherent Structures

LCS were calculated from the HFR observed surface currents using the FTLE metric. FTLE were calculated beginning with a velocity field over a selected time interval (in this case, 6 h). Then, from the derivative of the flow map the Cauchy-Green strain tensor field (C) and eigenvector field (λ_i) were computed to be used in Eq. (1):

$$S(x_0) = \left[\max_{i=N^{\lambda_i}}\left(C(x_0)\right)\right]^{1/2} \quad (1)$$

where $S(x_0)$ is the maximum stretching around point x_0. FTLE is then computed over a finite time (T)[10,79–81]. The resulting FTLE field changes in space and time with inputted HFR observed velocity field. These methods follow those in Veatch et al.[11].

Matching observed presence of null models to LCS

To associate krill and penguin presence with LCS, observations were matched in both space and time. LCS results were calculated each hour and at a 1 km spatial resolution to match the resolution of inputted HFR velocity data. Krill swarms and penguin locations were matched to the nearest hour of LCS map. This means that for the LCS results computed for 13:00 on January 15th, all krill and penguin location observations between 12:30 and 13:30 on January 15th were compared to the LCS results from 13:00. To match krill and penguin presence with LCS in space, a haversine function[82] was used to find the closest LCS result grid point (using the center of the grid point) to the krill or penguin location. The LCS value in that grid point for the LCS results on the nearest hour were associated with the krill or penguin observation. The same was done for null models.

Kolmogorov-Smirnov tests

Two-sample Kolomogorov-Smirnov (KS) tests[83] were used to determine if there are significant differences between the empirical distribution functions of observations and null models. KS tests are conducted using Eq. (2):

$$D = sup_x\left|F_{n,1}(x) - F_{n,2}(x)\right| \quad (2)$$

where D is the test statistic, $F_{n,1}(x)$ and $F_{n,2}(x)$ are the empirical distribution functions of the two samples. A small p-value from the KS test means that the two samples come from different distributions. One-sided KS tests are especially good at determining if the tails of two cumulative distributions are significantly different from each other.

Reporting summary

Further information on research design is available in the Nature Portfolio Reporting Summary linked to this article.

Data availability

Data and code used in this study are publicly available on NSF funded project SWARM's BCO-DMO site and GitHub. High Frequency Radar observed surface currents are available in the gap-filled version used in this study on BCO-DMO[84]. Lagrangian Coherent Structure Results for FTLE metrics are available on BCO-DMO[85]. EK80 acoustic data used to detect krill swarms are available on BCO-DMO ACROBAT data used to detect phytoplankton patches are available on BCO-DMO[86] Penguin GPS tag data are available University of Delaware's public archive (http://modata.ceoe.udel.edu/public/Antarctica_2020/SWARM_Penguin_CSVs/). Any questions can be directed to Jacquelyn Veatch (jveatch@whoi.edu).

Code availability

Code used to gap-fill High Frequency Radar data are available on GitHub (https://github.com/JackieVeatch/SWARM_CODAR). The code used to produce LCS results can be found on GitHub (https://github.com/JackieVeatch/SWARM_LCS). The code was modified from open-source MATLAB library[80] for use on HFR data. All other code for analysis can be found on GitHub (https://github.com/JackieVeatch/SWARM_analysis, https://github.com/JackieVeatch/SWARM_Krillanalysis, and https://github.com/JackieVeatch/SWARM_PenguinAnalysis). Any questions can be directed to Jacquelyn Veatch (jveatch@whoi.edu).

Received: 9 September 2024; Accepted: 5 February 2025;
Published online: 20 February 2025

References

1. Marquet, P. A. et al. Ecological and evolutionary consequences of patchiness: a marine-terrestrial perspective in *Patch dynamics* 277–304 (Berlin, Heidelberg: Springer Berlin Heidelberg, 1993).
2. Cheriton, O. M. et al. Effects of mesoscale physical processes on thin zooplankton layers at four sites along the west coast of the US. *Estuaries Coasts* **30**, 575–590 (2007).
3. Benoit-Bird, K. J. et al. Prey patch patterns predict habitat use by top marine predators with diverse foraging strategies. *PLoS ONE* **8**, e53348 (2013).
4. Genin, A. Bio-physical coupling in the formation of zooplankton and fish aggregations over abrupt topographies. *J. Mar. Syst.* **50**, 3–20 (2004).
5. Stommel, H. Varieties of oceanographic experience: the ocean can be investigated as a hydrodynamical phenomenon as well as explored geographically. *Science* **139**, 572–576 (1963).
6. Benoit-Bird, K. J. Resource patchiness as a resolution to the food paradox in the sea. *Am. Nat.* https://doi.org/10.1086/727473 (2023).
7. Mann, K. & Lazier, J. *Dynamics of Marine Ecosystems (3rd ed.)* (Wiley, 2013).
8. Power, J. H. Simulations of the effect of advective-diffusive processes on observations of plankton abundance and population rates. *J. Plankton Res.* **18**, 1881–1896 (1996).

9. Keister, J. E., Di Lorenzo, E., Morgan, C., Combes, V. & Peterson, W. Zooplankton species composition is linked to ocean transport in the Northern California current. *Glob. Change Biol.* **17**, 2498–2511 (2011).
10. Haller, G. Lagrangian coherent structures. *Annu. Rev. Fluid Mech.* **47**, 137–162 (2015).
11. Veatch, J. M., Kohut, J. T., Oliver, M. J., Statscewich, H. & Fredj, E. Quantifying the role of submesoscale Lagrangian transport features in the concentration of phytoplankton in a coastal system. *ICES J. Mar. Sci.* **81**, 760–773 (2024).
12. Lehahn, Y., d'Ovidio, F. & Koren, I. A satellite-based lagrangian view on phytoplankton dynamics. *Annu. Rev. Mar. Sci.* **10**, 99–119 (2018).
13. Lehahn, Y., d'Ovidio, F., Lévy, M. & Heifetz, E. Stirring of the northeast Atlantic spring bloom: a Lagrangian analysis based on multisatellite data. *J. Geophys. Res. - Oceans* **112**, C08005–C08005 (2007).
14. Hernández-Carrasco, I., Orfila, A., Rossi, V. & Garçon, V. Effect of small scale transport processes on phytoplankton distribution in coastal seas. *Sci. Rep.* **8**, 8613–8613 (2018).
15. Huhn, F., von Kameke, A., Pérez-Muñuzuri, V., Olascoaga, M. J. & Beron-Vera, F. J. The impact of advective transport by the South Indian Ocean Countercurrent on the Madagascar plankton bloom. *Geophys. Res. Lett.* **39**, n/a (2012).
16. Baudena, A. et al. Fine-scale structures as spots of increased fish concentration in the open ocean. *Sci. Rep.* **11**, 15805 (2021).
17. Emilie Tew, K. et al. Top marine predators track lagrangian coherent structures. *Proc. Natl. Acad. Sci. USA***106**, 8245–8250 (2009).
18. Fahlbusch, J. A. et al. Blue whales increase feeding rates at fine-scale ocean features. *Proc. R. Soc. B, Biol. Sci.* **289**, 20221180 (2022).
19. Goldbogen, J. A. et al. Mechanics, hydrodynamics and energetics of blue whale lunge feeding: efficiency dependence on krill density. *J. Exp. Biol.* **214**, 698–699 (2011).
20. Lomartire, S., Marques, J. C. & Gonçalves, A. M. M. The key role of zooplankton in ecosystem services: a perspective of interaction between zooplankton and fish recruitment. *Ecol. Indic.* **129**, 107867 (2021).
21. Maps, F. et al. Linking acoustics and finite-time L yapunov exponents reveals areas and mechanisms of krill aggregation within the G ulf of S t. L awrence, eastern Canada. *Limnol. Oceanogr.* **60**, 1965–1975 (2015).
22. St-Onge-Drouin, S., Winkler, G., Dumais, J.-F. & Senneville, S. Hydrodynamics and spatial separation between two clades of a copepod species complex. *J. Mar. Syst.* **129**, 334–342 (2014).
23. Fahlbusch, J. A. et al. Submesoscale coupling of krill and whales revealed by aggregative Lagrangian coherent structures. *Proc. R. Soc. B* **291**, 20232461 (2024).
24. Santora, J. A. et al. Krill space: a comparative assessment of mesoscale structuring in polar and temperate marine ecosystems. *ICES J. Mar. Sci.* **69**, 1317–1327 (2012).
25. Bernard, K. S. et al. Factors that affect the nearshore aggregations of Antarctic krill in a biological hotspot. Deep-Sea Res. Part I: Oceanogr. Res. Pap. **126**, 139–147 (2017).
26. Bernard, K. S. & Steinberg, D. K. Krill biomass and aggregation structure in relation to tidal cycle in a penguin foraging region off the Western Antarctic Peninsula. *ICES J. Mar. Sci.* **70**, 834–849 (2013).
27. Warren, J. D., Santora, J. A. & Demer, D. A. Submesoscale distribution of Antarctic krill and its avian and pinniped predators before and after a near gale. *Mar. Biol.* **156**, 479–491 (2009).
28. Nardelli, S. C. et al. Krill availability in adjacent Adélie and gentoo penguin foraging regions near Palmer Station, Antarctica. *Limnol. Oceanogr.* **66**, 2234–2250 (2021).
29. Pickett, E. P. et al. Spatial niche partitioning may promote coexistence of Pygoscelis penguins as climate-induced sympatry occurs. *Ecol. Evol.* **8**, 9764–9778 (2018).
30. Chapman, E. W., Hofmann, E. E., Patterson, D. L. & Fraser, W. R. The effects of variability in Antarctic krill (Euphausia superba) spawning behavior and sex/maturity stage distribution on Adélie penguin (Pygoscelis adeliae) chick growth: a modeling study. *Deep Sea Res. Part II: Topical Stud. Oceanogr.* **57**, 543–558 (2010).
31. Nicol, S. et al. Krill (Euphausia superba) abundance and Adélie penguin (Pygoscelis adeliae) breeding performance in the waters off the Béchervaise Island colony, East Antarctica in 2 years with contrasting ecological conditions. *Deep Sea Res. Part II: Topical Stud. Oceanogr.* **55**, 540–557 (2008).
32. Nowacek, D. P. et al. Super-aggregations of krill and humpback whales in Wilhelmina Bay, Antarctic Peninsula. *PLoS ONE* **6**, e19173 (2011).
33. Santora, J. A. & Reiss, C. S. Geospatial variability of krill and top predators within an Antarctic submarine canyon system. *Mar. Biol.* **158**, 2527–2540 (2011).
34. Santora, J. A., Reiss, C. S., Cossio, A. M. & Veit, R. R. Interannual spatial variability of krill (Euphausia superba) influences seabird foraging behavior near Elephant Island, Antarctica. *Fish. Oceanogr.* **18**, 20–35 (2009).
35. Fraser, W. R. & Trivelpiece, W. Z. Factors Controlling the Distribution of Seabirds: Winter-Summer Heterogeneity in the Distribution of Adélie Penguin Populations 257–272 (American Geophysical Union, Washington, D. C, 1996).
36. Emslie, S. D., Fraser, W., Smith, R. C. & Walker, W. Abandoned penguin colonies and environmental change in the Palmer Station area, Anvers Island, Antarctic Peninsula. *Antarct. Sci.* **10**, 257–268 (1998).
37. Schofield, O. et al. Penguin biogeography along the west Antarctic Peninsula: testing the canyon hypothesis with palmer LTER observations. *Oceanography* **26**, 204–206 (2013).
38. Fraser, W. R. & Trivelpiece, W. Z. Palmer LTER: relationships between variability in sea-ice coverage, krill recruitment, and the foraging ecology of Adélie penguins. *Antarct. J. U. S.* **30**, 271 (1995).
39. Fraser, W. R. & Trivelpiece, W. Z. Factors controlling the distribution of seabirds: Winter-summer heterogeneity in the distribution of Adélie penguin populations. *Found. Ecol. Res. West Antarct. Penins.* **70**, 257–272 (1996).
40. Kavanaugh, M. T. et al. Effect of continental shelf canyons on phytoplankton biomass and community composition along the western Antarctic Peninsula. *Mar. Ecol. Prog. Ser.***524**, 11–26 (2015).
41. Schofield, O. et al. Antarctic pelagic ecosystems on a warming planet. *Trends Ecol. Evol.* **39**, 1141–1153 (2024).
42. Root, T. L. & Schneider, S. H. Ecology and climate: research strategies and implications. *Science* **269**, 334–341 (1995).
43. Kohut, J. T. et al. Variability in summer surface residence time within a West Antarctic Peninsula biological hotspot. *Philos. Trans. R. Soc. Lond. Ser. A: Math., Phys., Eng. Sci.* **376**, 20170165–20170165 (2018).
44. Oliver, M. J. et al. Adélie penguin foraging location predicted by tidal regime switching. *PLoS ONE* **8**, e55163–e55163 (2013).
45. Carvalho, F., Kohut, J., Oliver, M. J. & Schofield, O. Defining the ecologically relevant mixed-layer depth for Antarctica's coastal seas. *Geophys. Res. Lett.* **44**, 338–345 (2017).
46. Hann, A. M., Bernard, K. S., Kohut, J., Oliver, M. J. & Statscewich, H. New insight into Salpa thompsoni distribution via glider-borne acoustics. *Front. Mar. Sci.* **9**, https://doi.org/10.3389/fmars.2022.857560 (2023).
47. Tarling, G. A. et al. Variability and predictability of Antarctic krill swarm structure. *Deep Sea Res. Part I: Oceanogr. Res. Pap.* **56**, 1994–2012 (2009).
48. Tarling, G. A. et al. Varying depth and swarm dimensions of open-ocean Antarctic krill Euphausia superba Dana, 1850 (Euphausiacea) over diel cycles. *J. Crustacean Biol.* **38**, 716–727 (2018).
49. Brierley, A. S. Diel vertical migration. *Curr. Biol.* **24**, R1074–R1076 (2014).
50. Padman, L., Erofeeva, S. Y. & Fricker, H. A. Improving Antarctic tide models by assimilation of ICESat laser altimetry over ice shelves. *Geophys. Res. Lett.* **35**, https://doi.org/10.1029/2008GL035592 (2008).

51. Della Penna, A., De Monte, S., Kestenare, E., Guinet, C. & d'Ovidio, F. Quasi-planktonic behavior of foraging top marine predators. *Sci. Rep.* **5**, 18063 (2015).
52. Berg, H. C. *Random Walks in Biology* (Princeton University Press, 1993).
53. Klafter, J. & Sokolov, I. M. Anomalous diffusion spreads its wings. *Phys. World* **18**, 29 (2005).
54. Okubo, A. & Levin, S. A. *Diffusion and Ecological Problems: Modern Perspectives*. Vol. 14 (Springer, 2001).
55. Nathan, R. et al. A movement ecology paradigm for unifying organismal movement research. *Proc. Natl. Acad. Sci. USA* **105**, 19052–19059 (2008).
56. Fraser, W. R. & Ainley, D. G. Ice edges and seabird occurrence in Antarctica. *BioScience* **36**, 258–263 (1986).
57. Wilson, R. P. et al. Luck in food finding affects individual performance and population trajectories. *Curr. Biol.* **28**, 3871–3877. e3875 (2018).
58. Hudson, K. et al. Reevaluating the canyon hypothesis in a biological hotspot in the Western Antarctic Peninsula. *J. Geophys. Res. Oceans* **124**, 6345–6359 (2019).
59. Carvalho, F. et al. Testing the canyon hypothesis: evaluating light and nutrient controls of phytoplankton growth in penguin foraging hotspots along the West Antarctic Peninsula. *Limnol. Oceanogr.* **65**, 455–470 (2019).
60. Hudson, K. et al. A recirculating eddy promotes subsurface particle retention in an antarctic biological hotspot. *J. Geophys. Res. Oceans* **126**, n/a (2021).
61. Prézelin, B. B., Hofmann, E. E., Moline, M. & Klinck, J. M. Physical forcing of phytoplankton community structure and primary production in continental shelf waters of the Western Antarctic Peninsula. *J. Mar. Res.* **62**, 419–460 (2004).
62. Dinniman, M. S. & Klinck, J. M. A model study of circulation and cross-shelf exchange on the west Antarctic Peninsula continental shelf. *Deep Sea Res. Part II: Topical Stud. Oceanogr.* **51**, 2003–2022 (2004).
63. Gorodetskaya, I. V. et al. Record-high Antarctic Peninsula temperatures and surface melt in February 2022: a compound event with an intense atmospheric river. *NPJ Clim. Atmos. Sci.* **6**, 202–218 (2023).
64. Vaughan, D. G. et al. Recent rapid regional climate warming on the Antarctic Peninsula. *Climatic Change* **60**, 243–274 (2003).
65. Hugh, W. D. et al. West Antarctic Peninsula: an ice-dependent coastal marine ecosystem in transition. *Oceanography***26**, 190–203 (2013).
66. Oliver, M. J. et al. Central place foragers select ocean surface convergent features despite differing foraging strategies. *Sci. Rep.* **9**, 157–157 (2019).
67. Statscewich, H. & Weingartner, T. A high-latitude modular autonomous power, control, and communication system for application to high-frequency surface current mapping radars. *IEEE* **54**, 1–3 (2012)
68. Kohut, J. Marine Technology; Study data from University of Alaska update understanding of marine technology (studying the impacts of local oceanographic processes on Adelie Penguin Foraging Ecology). *Ecol. Environ. Conserv.* **750**, 25–34 (2014).
69. Barrick, D. E., Evans, M. W. & Weber, B. L. Ocean surface currents mapped by radar. *Science***198**, 138–144 (1977).
70. Kohut, J. T., Roarty, H. J. & Glenn, S. M. Characterizing observed environmental variability with hf doppler radar surface current mappers and acoustic doppler current profilers: environmental variability in the coastal ocean. *IEEE J. Ocean. Eng.* **31**, 876–884 (2006).
71. Fredj, E., Roarty, H., Kohut, J., Smith, M. & Glenn, S. Gap filling of the coastal ocean surface currents from HFR data: application to the mid-atlantic bight HFR network. *J. Atmos. Ocean. Technol.* **33**, 1097–1111 (2016).
72. Veatch, J., Fredj, E. & Kohut, J. High Frequency Radars as Ecological Sensors: Using Lagrangian Coherent Structures to Quantify Prey Concentrating Features in *OCEANS 2022, Hampton Roads, Hampton Roads, VA, USA,* pp. 1–7. (2022)
73. De Robertis, A. & Higginbottom, I. A post-processing technique to estimate the signal-to-noise ratio and remove echosounder background noise. *ICES J. Mar. Sci.* **64**, 1282–1291 (2007).
74. Ryan, T. E., Downie, R. A., Kloser, R. J. & Keith, G. Reducing bias due to noise and attenuation in open-ocean echo integration data. *ICES J. Mar. Sci.* **72**, 2482–2493 (2015).
75. Reiss, C. S., Cossio, A. M., Walsh, J., Cutter, G. R. & Watters, G. M. Glider-Based estimates of meso-zooplankton biomass density: a fisheries case study on antarctic krill (Euphausia superba) around the northern antarctic peninsula. *Front. Mar. Sci.* **8**, 604043 (2021).
76. Luque, S.P. Diving Behaviour Analysis in R. *R News* **7**, 8–14 (2007)
77. Calenge, C. The package "adehabitat" for the R software: a tool for the analysis of space and habitat use by animals. *Ecol. Model.* **197**, 516–519 (2006).
78. Ainley, D. *The Adélie Penguin: Bellwether of Climate Change* (Columbia University Press, 2002).
79. Dosio, A., Vilà-Guerau de Arellano, J., Holtslag, A. A. M. & Builtjes, P. J. H. Relating eulerian and lagrangian statistics for the turbulent dispersion in the atmospheric convective boundary layer. *J. Atmos. Sci.* **62**, 1175–1191 (2005).
80. LCS tool: a computational platform for lagrangian coherent structures (<https://github.com/jeixav/LCS-Tool-Article/>).
81. Haller, G. Distinguished material surfaces and coherent structures in three-dimensional fluid flows. *Phys. D.* **149**, 248–277 (2001).
82. Distance calculation using Haversine formula (https://www.matchworkds.com/matlabcentral/fileexchange/27785-distance-calculation-suing-haversine-formula, 2024).
83. Massey, F. J. Jr The Kolmogorov-Smirnov test for goodness of fit. *J. Am. Stat. Assoc.* **46**, 68–78 (1951).
84. Veatch, J., Klinck, J. M., Oliver, M., Statscewich, H., Kohut, J. High Frequency Radar (HFR) observed surface currents at Palmer Deep Canyon in the coastal ocean west of the Antarctic Peninsula in 2020 *BCO-DMO* version 1, https://doi.org/10.26008/1912/bco-dmo.917884.1 (2024).
85. Veatch, J., Klinck, J. M., Oliver, M., Statscewich, H., Kohut, J. Results from Finite Time Lyapunov Exponent calculations using High Frequency Radar observed surface currents around Palmer Deep Canyon from January to March of 2020 *BCO-DMO*version 1, https://doi.org/10.26008/1912/bco-dmo.917914.1 (2024).
86. Bernard, K. S., Hann, A., Veatch, J. Krill swarms detected with active acoustic EK80 onboard small boat surveys in Palmer Deep Canyon, Antarctica during January-March 2020 *BCO-DMO* version 1, https://doi.org/10.26008/1912/bco-dmo.949922.1 (2025).

Acknowledgements

This project was funded through the National Science Foundation, award # OPP 1745009. Many thanks to the Antarctic Support Contractor and their teams aboard the ARSV Laurence M. Gould, at Palmer Station, and headquarters in Denver, CO without whom a study of this scale would not be possible. Thank you to the students and field assistants for their valued involvement in the SWARM project in particular, Dr. Katherine Gallagher, Dr. Jerome Pinti, Dr. Thilo Klenz, Ethan Handel, and Jordi Maisch. We thank the Palmer Long-Term Ecological Research team and the Commission for the Conservation of Antarctic Marine Living Resources for their advice and collaboration, in particular the Seabird team of the Palmer Long-Term Ecological Research who were instrumental in the deployment of penguin tags.

Author contributions

J.V. contributed by writing the original draft of this manuscript, leading the formal analysis, validation and visualization of data, and contributed equally

to data curation, developing methodology, and the conceptualization of this manuscript. J.K. contributed by leading the funding acquisition and supervision of this manuscript and contributed equally to the conceptualization, data acquisition, development of methodology, and reviewing and editing of this manuscript. M.O. contributed equally to data acquisition, development of methodology, analysis, and reviewing and editing of this manuscript, led the visualization of penguin tagged data, and contributed supporting supervision. H.S. contributed a leading role to the data acquisition and contributed equally to the conceptualization of this manuscript. E.F. contributed equally to the conceptualization and development of methodology in this manuscript and contributed supporting supervision. K.B. contributed equally to data validation, conceptualization, development of methodology, and reviewing and editing of this manuscript. H.F. contributed equally to conceptualization and reviewing and editing of this manuscript. W.F. contributed to penguin foraging data acquisition, conceptualization, reviewing and editing of this manuscript. A.H. led the validation of the active acoustic data and contributed equally to reviewing and editing of this manuscript. G.V. led the validation of the penguin tagged data and contributed equally to reviewing and editing of this manuscript.

Competing interests

The authors declare no competing interests.

Additional information

Supplementary information The online version contains supplementary material available at https://doi.org/10.1038/s43247-025-02101-x.

Correspondence and requests for materials should be addressed to Jacquelyn M. Veatch.

Peer review information *Communications Earth & Environment* thanks Alberto Baudena and the other, anonymous, reviewer(s) for their contribution to the peer review of this work. Primary Handling Editors: Heike Langenberg, Aliénor Lavergne. A peer review file is available.